An approximately H^1-optimal Petrov-Galerkin meshfree method: application to computation of scattered light for optical tomography

N Pimprikar[1], J Teresa[2], D Roy[1,3], R M Vasu[4], K Rajan[4]

Abstract: Nearly pollution-free solutions of the Helmholtz equation for k-values corresponding to visible light are demonstrated and verified through experimentally measured forward scattered intensity from an optical fiber. Numerically accurate solutions are, in particular, obtained through a novel reformulation of the H^1 optimal Petrov-Galerkin weak form of the Helmholtz equation. Specifically, within a globally smooth polynomial reproducing framework, the compact and smooth test functions are so designed that their normal derivatives are zero everywhere on the local boundaries of their compact supports. This circumvents the need for *a priori* knowledge of the true solution on the support boundary and relieves the weak form of any jump boundary terms. For numerical demonstration of the above formulation, we used a multimode optical fiber in an index matching liquid as the object. The scattered intensity and its normal derivative are computed from the scattered field obtained by solving the Helmholtz equation, using the new formulation and the conventional finite element method. By comparing the results with the experimentally measured scattered intensity, the stability of the solution through the new formulation is demonstrated and its closeness to the experimental measurements verified.

Keywords: H^1 optimality; meshfree methods; Helmholtz equation; numerical pollution; optical tomography

---

[1] Computational Mechanics Lab, Department of Civil Engineering, Indian Institute of Science, Bangalore 560012, India

[2] Department of Physics, Indian Institute of Science, Bangalore 560012, India

[3] Communicating author; Email: royd@civil.iisc.ernet.in

[4] Department of Instrumentation and Applied Physics, Indian Institute of Science, Bangalore 560012, India

1   Introduction

There are a number of application areas where time harmonic wave propagation modeled by the Helmholtz equation needs to be solved repeatedly [Devaney(1982), Bao, Wei and Zhao(2004), William(1984)]. These include acoustic tomography with application in oil prospecting, optical diffraction tomography for cross-sectional imaging of fiber and integrated optics wave-guides and antenna design in electro-magnetics. The boundary value problem represented by $\Delta u(r) + k^2 u(r) = -f(r)$, where $f(r)$ is a harmonic source and k the wavenumber, results in highly oscillatory solutions for large k. Therefore if a solution is sought through the conventional finite element (FE) discretization, the characteristic mesh size h may have to be made impracticably small to resolve the oscillations. One way of getting at an acceptable h could be to demand that $kh =$ constant, resulting in constant grid spacing throughout the domain. Insisting on a constant kh, when k is a large precipitates a non-robust behavior of the FE solution, known as the pollution effect [Babuška and Sauter, (2000),Bao, Wei and Zhao (2004)]. Many in the past have recognized this difficulty and worked on means to extracting acceptably stable solutions. One of the approaches has been to refine the FE method through its so-called *h and h − p* versions [Ihlenburg and Babuška (1995), Ihlenburg and Babuška (1997)]. Another approach involves the reformulation of the problem using a boundary integral equation (BIE) enriching also the approximation space with plane waves or spheroidal wave functions (instead of only piece-wise continuous polynomials) which are helpful in capturing the large k behaviour of the solution [Monk and Wang (1999)]. In Qian *et al.* [Qian, Han, Ufimtsev and Atluri (2004), Qian, Han and Atluri (2013)], using vector test functions constructed from gradients of the fundamental solution of the Helmholtz equation, a non-hyper-singular BIE is arrived at for the gradient of the sought after solution. A regularized version of the above non-hyper-singular BIE is solved through a collocation scheme, the numerical implementation of which is speeded up by novel interpolation called the fast multipole method. Thus the above scheme involves only O(N) computations thus making it able to tackle practical problems of large dimension. In [Bruno, Geuzaine and Reitich (2004)], following the high frequency integral equation formulation, the rapidly oscillating surface waves are captured with a relatively coarse discretization. A wavelet collocation method involving the discrete convolution algorithm is discussed in [Bao, Wei and Zhao (2004)], wherein it is shown through Fourier analysis that wavelet-based algorithm is essentially pollution free. In the context of the inverse problem of recovery of spatial inhomogeneities in $k(r)$, efficient time-marching schemes are suggested and implemented to solve the Helmholtz equation with and without first order paraxial or parabolic approximation [Natterer (2003)].

The present work is concerned with the exploitation of a smooth, polynomial re-

producing functional discretization scheme within a nearly H^1 optimal Petrov-Galerkin weak formulation towards obtaining a numerically accurate solution to the Helmholtz equation with moderate to high wave numbers. The standard Galerkin projection, based on an orthogonalization of the residual field with respect to a finite dimensional functional approximation space, yields the best approximation property (in the form of minimum energy norm or H^1 semi-norm) for Laplace's equation and performs consistently with varying mesh resolutions. This is however not the case with the Helmholtz operator, wherein considerable numerical pollution could occur, especially for large wave numbers that precipitate the relative dominance of the advection or derivative-free terms over the Laplacian term, as the above best approximation property is no longer satisfied. The so-called pollution effect is typically manifested in the numerical simulations through the presence of sharp gradient layers and spuriously high-frequency oscillations [Ihlenburg and Babuska (1995)]. The pollution effect simultaneously gives rise to dispersion [Babuska, Ihlenburg, Paik and Sauter (1995)] as the wave number of the 'exact' solution is different from that of the discretized numerical solution. Based on the conventional Galerkin approximation, a condition like $kh < 1$ (where h denotes the discretization step-size) may be enforced towards obtaining acceptable numerical accuracy and, if domain discretization is, for instance, through the finite element method (FEM), this could entail an impracticably dense meshing for large k [Ihlenburg and Babuška (1995)]. A similar scenario arises with meshfree methods wherein a high particle (nodal) density must be used. While this warrants a significant increase in the system dimension post-discretization and might possibly yield acceptably accurate solutions for not-so-large k, the best approximation property is nevertheless not restored.

Significant research efforts have been invested in alleviating the numerical issues mentioned above. Yet, there is hardly an efficient method that completely circumvents the above problem and hence Zienkiewicz [2000] puts this problem in the category of unsolved ones. Galerkin's least-square (GLS) method [Harari and Hughes (1992)] is one such stabilization scheme that completely avoids the pollution effect in one-dimension. Unfortunately this method is far less effective in two or still higher dimensions. A quasi-stabilized finite element method (QSFEM) has been proposed by Babuska, Ihlenburg, Paik and Sauter [1995], which attempts at addressing the pollution effect in 2D problems. But the efficacy of this method to non-homogeneous problems and those involving non-uniform meshes as well as higher order interpolations is unclear. Other methods aimed at reducing the pollution effect include residual-free bubble (RFB) based approaches [Brezzi, Franca and Russo (1998), Franca, Neslliturk and Stynes (1998)], residual-based finite element method (RBFEM) [Oberai and Pinsky (2000)], streamlined upwind Galerkin

methods (SUPG) [Brooks and Hughes (1982)], generalized finite element method (GSFEM) [Strouboulis, Babuska and Copps (2000)] and the discontinuous enrichment method (DEM) [Farhat, Harari and Franca (2001)]. Of specific interest in this work is the nearly optimal Petrov-Galerkin method [Barbone and Harari (2001)], which is based on approximately enforcing the optimal H^1 semi-norm of the error *en route* to the numerical determination of the solution. While the last method has been demonstrated to be nodally exact for the 1D Helmholtz equation, an efficacious implementation of the scheme for 2D and still higher dimensions remains somewhat elusive. The major obstacle in deriving an accurate test (weight) function within an H^1 optimal Petrov-Galerkin scheme seems to be the prior lack of knowledge of the true error (that in turn necessitates prior knowledge of the true solution) appearing in the boundary integral of the weak form.

The boundary integral appearing in the H^1 optimal Petrov-Galerkin weak form also contains a jump term involving the difference of the normal derivatives of the test and trial functions. However, given the higher order global smoothness and compactness of the shape functions within a meshfree functional discretization scheme, it appears worthwhile to derive the H^1 optimal Petrov-Galerkin approach based on such smooth test functions so constructed that their normal derivatives identically vanish on the boundary (interior or otherwise) thereby driving the boundary term to zero. This would simplify the formulation by eliminating the boundary term. Moreover, if the shape functions are constructed based on the condition of polynomial reproduction, it is also likely to bring in higher numerical accuracy vis-à-vis the FEM. With the rapid progresses made in the development of meshfree methods, there is a large family of such approximation methods to choose from, e.g. moving least-square Petrov-Galerkin method (MLPG) [Atluri and Zhu (1998), Atluri, Han and Rajendran (2004)], element-free Galerkin method (EFG) [Lu, Belytschko, Gu (1994)], partition of unity method (PUM) [Babuska and Melenk (1997), Melenk and Babuska(1996)], the $h - p$ cloud method [Duarte and Oden (1996)], reproducing kernel particle methods (RKPM) [Liu, Jun, Li, Adee and Belytschko (1995), Liu, Jun, and Zhang (1995)], moving least square kernel method (MLSRK) [Liu, Li and Belytschko (1997), Chen, Pan, Wu and Liu (1996)], smooth particle hydrodynamics [Swegle, Hicks and Attaway (1995):], the point interpolation method[Liu and Gu(2001)] to name a few. In this work, however, an error reproducing kernel method (ERKM) [Shaw, Banerjee and Roy (2008), Shaw, Bendapudi and Roy (2008), Shaw and Roy (2007, 2008)] is adopted, wherein non-uniform rational B-splines (NURBS) are employed as bases in the initial (zeroth order) functional approximation followed by a representation of the resulting approximation error through polynomial reproduction.

The rest of the paper is organized as follows. Section 2 describes the ERKM-based

functional approximation scheme for completeness. In Section 3, the approximate H^1 optimal weak formulation is outlined with emphasis on the derivation of the test function based on a least square minimization. Application of the resulting Petrov-Galerkin scheme to the Helmholtz equation, as it arises in the forward problem of diffraction tomography, is dwelt upon in Sections 4 and 5. Here, we also compare the forward solution with the experimentally measured scattered field from an optical fiber. Finally, in Section 6, a few concluding remarks are provided.

2 NURBS-based ERKM

With a view to combining the global smoothness of meshfree methods with the popularly adopted meshbased discretization of the FEM, several NURBS-based hybrid methods, e.g. error reproducing kernel method (ERKM) [Shaw and Roy (2007)] and parametric mesh-free methods [Shaw and Roy (2008)] have been developed. The NURBS based parametric bridging gives smooth solutions with shape functions reproducing polynomials of appropriate degrees and derivatives of shape functions reproducing derivatives of these polynomials. A NURBS based parametric bridging method uses an appropriate tensor product of NURBS bases as the kernel function in deriving the shape functions via polynomial reproduction. The FEM-like meshing is necessitated in the construction of the NURBS bases and the derivation of the shape function relies upon a family of piecewise bijective geometric maps between subsets of the original domain and a rectangular (cuboidal) parametric domain These methods have been successfully applied to several linear and nonlinear problems of general interest in solid mechanics. They however have limitations for highly irregular geometries, wherein the geometric map might precipitate ill-conditioning in the discretized weak form. Another problematic issue is a possible non-conformality in the numerical integration owing to the dual use of knots as particles (or nodes) whilst constructing the NURBS or B-spline bases. A significant extension and improvement of this concept, addressing most of these issues by replacing the NURBS (B-splines) with triangular B-splines has also been reported [Sunilkumar and Roy (2010) Sunilkumar, Roy and Reid (2012)]

The ERKM method is briefly described below. Some details on the NURBS bases are given in Appendix-I. Here, to begin with, the target function is directly approximated through NURBS basis functions. However, NURBS basis functions do not reproduces polynomials (except for the constant or linear ones). One thus formally defines an error function, which is made to meet the polynomial reproduction condition via a non-NURBS family of basis functions. The functional approximation is finally obtained by adding the approximated error function to the NURBS approximation. For a more detailed exposition, refer to [Shaw and Roy (2007, 2008), Shaw, Banerjee and Roy (2008)].

2.1 *ERKM shape functions*

Let $u(\mathbf{x})$, $\mathbf{x} \in \mathbf{R}^d$, denote a scalar-valued continuous function defined on a simply connected open set $\Omega \subset \mathbf{R}^d$ with a Lipschitz continuous boundary $\partial\Omega$ and $P_p = P_p(\Omega)$ vector space of polynomials of degree $\leq p$ on Ω where p is the highest degree of polynomials to be reproduced. The dimension of P_p is $\frac{(p+d)!}{p!d!}$. Multi-index notations are adopted here. Thus, defining the multi-index $\alpha = (\alpha_1, \alpha_2, ..., \alpha_d)$ to be an q- tuple of non-negative integers α_j and its length $|\alpha| = \sum_{i=1}^{q} \alpha_i$, the αth derivative of $u(\mathbf{x})$ is written as $D^\alpha u(\mathbf{x}) = \partial_{x_1}^{\alpha_1} \partial_{x_2}^{\alpha_2}...\partial_{x_q}^{\alpha_q} u(\mathbf{x})$. Moreover, one defines $\alpha! = \alpha_1!\alpha_2!...\alpha_q!$ and $x^\alpha = x_1^{\alpha_1} x_2^{\alpha_2}...x_q^{\alpha_q}$. Let $\bar{\Omega} = \Omega \cup \partial\Omega$ be discretized by set of N_p particles or nodes $\{\{\mathbf{x}_i\}_{i=1}^{N_p}\} \subset \bar{\Omega}$. Associated with them is a set of discretized function values $\{u_i \overset{\Delta}{=} u(\mathbf{x}_i)\}_{i=1}^{N_p}$. Now the initial approximation of the function is given by:

$$u_{bs}^a(\mathbf{x}) = \sum_{i=1}^{N_p} R_i^p(\mathbf{x}) u_i \qquad (1)$$

where $R_i^p(\mathbf{x})$ is a B-spline (or NURBS) basis function of the degree p and $u_{bs}^a(\mathbf{x})$ denotes the B-spline approximation of $u(\mathbf{x})$. The accruing (notional) error owing to this approximation is then reproduced via non-B-spline family of functions $\{\bar{\Psi}_i(\mathbf{x})\}$ such that:

$$u(\mathbf{x}) - u_{bs}^a(\mathbf{x}) = \sum_{i=1}^{N_p} \bar{\Psi}(\mathbf{x}) u_i \qquad (2)$$

where

$$\Psi_i(\mathbf{x}) = R_i^p(\mathbf{x}) + \bar{\Psi}_i(\mathbf{x}) \qquad (3)$$

$\Psi_i(\mathbf{x})$ is the ERKM shape function corresponding to the ith particle. The function $\bar{\Psi}_i(\mathbf{x})$ may be written as

$$\bar{\Psi}_i(\mathbf{x}) = C(\mathbf{x} - \mathbf{x}_i)\varphi_{a_i}(\mathbf{x} - \mathbf{x}_i) \qquad (4)$$

where $\varphi_{a_i}(\mathbf{x} - \mathbf{x}_i)$ is a compactly supported kernel function (also referred to as weight or window function) with $a_i \in \mathbf{R}^+$ denoting the dilation parameter. The correction function $C(\mathbf{x} - \mathbf{x}_i)$ is given by:

$$C(\mathbf{x} - \mathbf{x}_i) = H^T(\mathbf{x} - \mathbf{x}_i)\bar{\mathbf{b}}(\mathbf{x}) \qquad (5)$$

where $H^T(\mathbf{x} - \mathbf{x}_i) = \{(\mathbf{x} - \mathbf{x}_i)^\alpha\}_{|\alpha| \leq p}^T$ is the set of monomial basis functions and $\bar{\mathbf{b}}(\mathbf{x}) = \{\bar{b}_\alpha(\mathbf{x})\}_{|\alpha| \leq p}$

is the set of coefficient functions that may be interpreted as moving with the locations **x** of the approximation. From equations (3), (4), (5), $\Psi_i(\mathbf{x})$ may be written as

$$\Psi_i(\mathbf{x}) = R_i^p(\mathbf{x}) + \bar{H}^T(\mathbf{x} - \mathbf{x}_i)\bar{\mathbf{b}}(\mathbf{x})\varphi_{a_i}(\mathbf{x} - \mathbf{x}_i) \tag{6}$$

$\bar{\mathbf{b}}(\mathbf{x})$ can be found from the reproducing conditions:

$$\sum_{i=1}^{N_P} \Psi_i(\mathbf{x})\mathbf{x}_i^\alpha = \mathbf{x}^\alpha, |\alpha| \leq p \tag{7}$$

$$\Rightarrow \sum_{i=1}^{N_P} \Psi_i(\mathbf{x})(\mathbf{x} - \mathbf{x}_i)^\alpha = \delta_{|\alpha|,0}, |\alpha| \leq p \tag{8}$$

$$\Rightarrow \mathbf{M}(\mathbf{x})\bar{\mathbf{b}}(\mathbf{x}) = \mathbf{H}(0) - \sum_{i=1}^{N_p} R_i^p(\mathbf{x})\mathbf{H}(\mathbf{x} - \mathbf{x}_i) \tag{9}$$

Thus $\bar{\mathbf{b}}(\mathbf{x})$ is given as

$$\bar{\mathbf{b}}(\mathbf{x}) = \mathbf{M}^{-1}(\mathbf{x})\left[\mathbf{H}(0) - \sum_{i=1}^{N_p} R_i^p(\mathbf{x})\mathbf{H}(\mathbf{x} - \mathbf{x}_i)\right] \tag{10}$$

$\mathbf{M}(\mathbf{x})$ is called as moment matrix and is given as

$$\mathbf{M}(\mathbf{x}) = \sum_{i=1}^{N_p} \mathbf{H}(\mathbf{x} - \mathbf{x}_i)\mathbf{H}^T(\mathbf{x} - \mathbf{x}_i)\varphi_{a_i}(\mathbf{x} - \mathbf{x}_i) \tag{11}$$

Hence, ERKM shape functions may finally be expressed as

$$\Psi_i(\mathbf{x}) = R_i^p(\mathbf{x}) + \left[\mathbf{H}(0) - \sum_{i=1}^{N_P} R_i^p(\mathbf{x})\mathbf{H}(\mathbf{x} - \mathbf{x_i})\right]^T \mathbf{M}^{-1}(\mathbf{x})\mathbf{H}(\mathbf{x} - \mathbf{x_i})\varphi_{a_i}(\mathbf{x} - \mathbf{x_i}) \tag{12}$$

3 An approximately H^1 optimal formulation

Consider the following boundary value problem: find $u : \bar{\Omega} \to C$ such that

$$Lu = f \text{ in } \Omega \subset \mathbb{R}^d \tag{13}$$

$$u = 0 \text{ on } \partial\Omega \tag{14}$$

Here $f : \bar{\Omega} \to C$ is the given source function, L a non-Laplacian linear differential operator (e.g. a Laplacian term plus an advection term) and u the unknown function. Homogenous boundary conditions are chosen only for the sake of expositional

simplicity. Generalizations to non-homogenous and other types of boundary conditions (Neumann/Robin) would follow a similar procedure. For the variational formulation, the variation $w = \delta u$ (or equivalently the test function in the weak form) must satisfy $w = 0$ on $\partial\Omega \, \forall \, w \in V$; where $V \subset H^1_0(\Omega)$. In the conventional Galerkin setting, one typically aims at finding $u \in H^1(\Omega)$ such that $\forall w \in V$

$$\tilde{a}(w,u) = L(w) \tag{15}$$

where

$$\tilde{a}(w,u) = (w, Lu) \quad = (L^*w, u) \tag{16}$$

is a bilinear form for all $u \in H^1(\Omega), w \in V$ and $L(w) = (w, f)$ is the so called linear form. Upon integration by parts applied to the Laplacian (diffusion) term, the LHS of the above equation may be reduced to the canonical bilinear form, henceforth referred to as $a(w,u)$. Note that L^* denotes the adjoint of differential operator L and $(.,.)$ is the standard inner product with $f \in L^2(\Omega)$.

Given the special form of Dirichlet boundary condition (i.e. $u = 0$ on $\partial\Omega$), we will henceforth assume that u and w (or their finite dimensional approximations $\bar{u}$ and $\bar{w}$) are drawn from the same function space. Now, if one were to adopt a mesh-based discretization technique (e.g. the FEM), the canonical weak form may be written as:

$$a(\bar{w}, \bar{u}) = L(\bar{w}) \tag{17}$$

where $\bar{u}, \bar{w} \in \bar{V} \subset V$ with $\bar{V}$ denoting the finite dimensional vector space spanned by FEM-based basis functions, typically with C^0 continuity. However, as noted before, the approximation $\bar{u}$ solving the above weak form need not be optimal in any sense. In order to enforce the H^1 optimality, which seems to be a natural goal given the Sobolev space setting, Barbone and Harari (2001) have proposed an alternative formulation for the weak form. Here the problem is to find $\bar{u} \in \bar{V}$ such that $\forall \bar{w} \in \bar{V}$, the following identity must be enforced:

$$(\nabla\bar{w}, \nabla e) = 0 \tag{18}$$

where e is the signed difference between the approximate and exact (true) solutions, i.e.

$$e = \bar{u} - u \tag{19}$$

One cannot directly invert the above weak form for $\bar{u}$ as the true solution u is not known. Using Equation (15) and (16), it has however been argued [Barbone and

Harari (2001)] that, by way of enforcing the H^1 optimality, one may adopt an unsymmetric (Petrov-Galerkin) weak form wherein the test function $\tilde{w} \in \tilde{V} \subset V$ satisfies the adjoint problem for every $\bar{w} \in \bar{V}$:

$$L^* \tilde{w} = \nabla^2 \tilde{w} \quad in \quad \Omega^{'} \quad and \tag{20}$$

$$\tilde{w} = w \quad in \quad \partial\Omega^{'} \tag{21}$$

Here $\Omega^{'} = \cup \Omega^e$ is the domain interior and $\partial\Omega^{'} = \cup \partial\Omega^e$ the collection of all boundaries, interior as well and exterior. Here Ω^e is the open interior of the element e and $\partial\Omega^e$ its boundary.

After integration by parts, Equation (18) is reduced to

$$(\nabla\bar{w}, \nabla e) = - (\nabla^2 \bar{w}, e)_{\Omega'} + ([\bar{w}_{,n}], e)_{\partial\Omega'} \tag{22}$$

Here $[\bar{w}_{,n}]$ is the jump term defined as

$[\bar{w}_{,n}] = \left[\frac{\partial \bar{w}}{\partial n}\right] = \frac{\partial \bar{w}^+}{\partial n^+} + \frac{\partial \bar{w}^-}{\partial n^-}$, the superscripts+ and - indicate approaching the element boundary from +and - sides, respectively. Using Equation (20) in (22), we may write:

$$(\nabla\bar{w}, \nabla e) = - (L^* \tilde{w}, e)_{\Omega'} + ([\bar{w}_{,n}], e)_{\partial\Omega'} \tag{23}$$

Integrating the first term on the RHS of the above identity by parts (which yields the canonical bilinear form $a(\tilde{w}, e)$ and a boundary term), one obtains:

$$(\nabla\bar{w}, \nabla e) = a(\tilde{w}, e) + ([\bar{w}_{,n} - \tilde{w}_{,n}], e)_{\partial\Omega'} \tag{24}$$

Considering $\tilde{V} \subset V$, using the definition (19) and finally invoking the canonical weak form $a(\tilde{w}, u) - L(\tilde{w}) = 0$, we get

$$(\nabla\bar{w}, \nabla e) = a(\tilde{w}, \bar{u}) - L(\tilde{w}) + ([\bar{w}_{,n} - \tilde{w}_{,n}], e)_{\partial\Omega'} \tag{25}$$

The above equation thus suggests the following Petrov-Galerkin formulation: find $\bar{u} \in \bar{V} \; \forall \; \tilde{w} \in \tilde{V}$, such that

$$a(\tilde{w}, \bar{u}) = L(\tilde{w}) \tag{26}$$

Referring to Equation (22), one observes that the solution $\bar{u}$ obtained by inverting the weak form (23), should satisfy:

$$(\nabla\bar{w}, \nabla e) = ([\bar{w}_{,n} - \tilde{w}_{,n}], e)_{\partial\Omega'} \tag{27}$$

In other words, the condition $(\nabla\bar{w}, \nabla e) = 0$ enforcing H^1 optimality is met provided that either the jump terms in the RHS of Equation (27) identically vanish or that

$\bar{w}_{,n} - \tilde{w}_{,n} = 0$ identically on $\partial\Omega'$. However, with the FEM-based functional approximations being only C^0, such jump terms on $\partial\Omega'$ would almost always remain non-zero thereby frustrating efforts at imposing the desired optimality condition in a precise manner. This justifies the use of the phraseology 'nearly-optimal' in [Barbone and Harari (2001)], whilst describing the FEM-based implementation of the method. In this context, a mesh-free or hybrid discretization, which provides for higher order smoothness in the shape functions, is of great use as the jump terms over $\partial\Omega'$ are no longer present and this should enable a more precise numerical enforcement of the H^1 optimality condition. Thus, if we specifically adopt the ERKM based approach and denote the NURBS cells as elements (i.e. Ω_e denoting the interior of the eth NURBS cell and $\partial\Omega_e$ its boundary), then one need only to solve the following PDE to determine the test function $\tilde{w}$:

$$L^*\tilde{w} = \nabla^2\bar{w} \quad on \quad \Omega_e \tag{28}$$

$$\tilde{w} = \bar{w} \quad on \quad \partial\Omega_e \tag{29}$$

3.1   Evaluating the test function

While the ERKM approximation scheme is based on an FE-like meshing of the domain, most meshfree methods bypass such meshing and obtain the functional approximation purely based on a set of (randomly) scattered nodes. We conform to this general plan of meshfree discretization in describing the derivation of the test function $\tilde{w}$. Let Ω_i denote the interior of the support of the ith shape function that necessarily contains the ith node. Let $\partial\Omega_i$ denote the boundary of Ω_i. Since supports of both $\tilde{w}_i$ and $\bar{w}_i$ are taken to coincide with $\bar{\Omega}_i$, Equations (20) and (21), restricted to Ω_i, may be written in an uncoupled manner (with respect to similar such equations corresponding to node j, where $j \neq i$) as:

$$L^*\tilde{w}_i = \nabla^2\bar{w}_i \quad on \quad \Omega_i \tag{30}$$

$$\tilde{w}_i = w_i \quad on \quad \partial\Omega_i \tag{31}$$

Letting $\bar{w}_i = N_i$, where N_i denotes the ith shape function (e.g. the ith ERKM-based shape function), we get:

$$L^*\tilde{w}_i = \nabla^2 N_i \quad on \quad \Omega_i \tag{32}$$

$$\tilde{w}_i = N_i \quad on \quad \partial\Omega_i \tag{33}$$

Thus, $\tilde{w}_i - N_i$ typically corresponds to a bubble function [Oberai and Pinsky (2000), Brezzi, Franca and Russo (1998), Franca, Neslirurk and Stynes (1998)] (which is

presently at least C^1 or still higher order continuous uniformly overΩ) in $\Omega_i$for every i. A direct inversion of Equations (32) and (33) is however not quite desirable as the computational effort needed would be commensurate with the original problem itself. In this work, a simpler strategy based on a least square minimization is suggested to arrive at $\tilde{w}_i$. In particular, we adopt the following form for$\tilde{w}_i - N_i$:

$$\tilde{w}_i - N_i = c_i B_i(x,y) \tag{34}$$

where c_i is a yet-undetermined constant and $B_i(x,y)$ a $C_0^\infty(\Omega)$ bubble function, compactly supported over Ω_i and presently assumed to be of the form:

$$B_i(x,y) = \exp\left(\frac{-a^2}{a^2 - x^2}\right) \times \exp\left(\frac{-b^2}{b^2 - y^2}\right) \tag{35}$$

Here a and b are the dimensions of Ω_i,which is rectangular for $d = 2$ (cuboidal for$d > 2$) for the ERKM shape function. Figure 1 shows the geometry of Ω_i and the associated bubble function $B_i(x,y)$.

Now, substituting $\tilde{w}_i = C_i B_i(x,y) + N_i$ in Equation (30), one obtains:

$$L^*(c_i B_i(x,y) + N_i) \approx \nabla^2 N_i \tag{36}$$

where the pointwise equality is now only valid approximately. Denoting by R_i, the residual of the above equation, i.e.

$$R_i = L^*(c_i B_i(x,y) + N_i) - \nabla^2 N_i, \tag{37}$$

one may determine c_i through a least square minimization of the $L^2(\Omega_i)$ norm of R_i. Specifically, one has the following one dimensional linear algebraic equation to determine$c_i$for every node i:

$$\frac{d}{dc_i} \int\limits_{\Omega_i} (R_i)^2 d\Omega_i = 0 \quad or \tag{38a}$$

$$\frac{d}{dc_i} \int\limits_{\Omega_i} \left[L^*(c_i B_i(x,y) + N_i) - \nabla^2 N_i\right]^2 d\Omega_i = 0 \tag{38b}$$

As noted above, the integration is performed over$\Omega_i \equiv \sup p(N_i)$, which is the same assup $p(B_i)$. The identical supports for the bubble and shape functions also help identically satisfying the boundary condition in Equation (33). Typical supports of B_i (and henceN_i) are shown in Figures 1(a) and 1(b).

(a) Domain of the shape function of node

(b) Bubble function for node
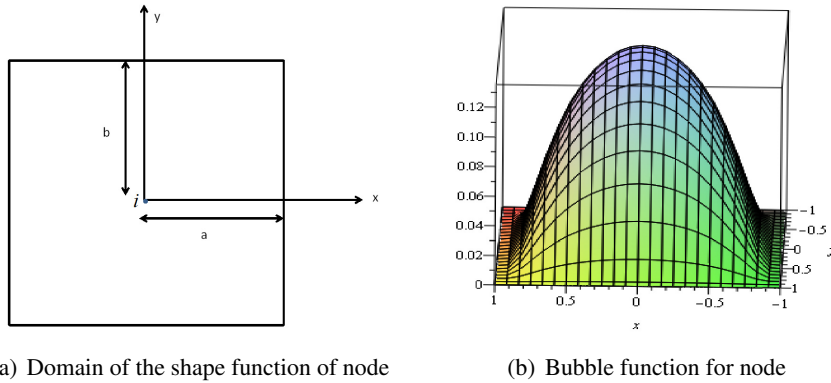
Figure 1:

Of specific interest in this work is the evaluation of the set of constants $\{c_i\}$ for the Helmholtz equation:

$$\nabla^2 u + k^2 u = 0 \quad in \quad \Omega \tag{39}$$

$$u = \bar{u} \quad in \quad \partial\Omega \tag{40}$$

Here, the self-adjoint differential operator L is identical to its adjoint L^*:

$$L \equiv L^* \equiv \nabla^2 + k^2 I \tag{41}$$

where I denotes the identity operator. Substituting (41) into (38b) we get,

$$\frac{d}{dc_i} \int_{\Omega_i} \left[(\nabla^2 + k^2)(c_i B_i + N_i) - \nabla^2 N_i \right]^2 d\Omega_i = 0 \tag{42}$$

i.e.

$$\int_{\Omega_i} \frac{d}{dc_i} \left[(\nabla^2 + k^2)(c_i B_i + N_i) - \nabla^2 N_i \right]^2 d\Omega_i = 0 \tag{43}$$

which finally yields:

$$c_i = \frac{ - \int_{\Omega_i} k^2 N_i \left[\nabla^2 B_i + k^2 B_i \right] d\Omega_i }{ \int_{\Omega_i} \left[\nabla^2 B_i + k^2 B_i \right] \left[\nabla^2 B_i + k^2 B_i \right] d\Omega_i } \tag{44}$$

Given the general infeasibility of analytical integration, the constants $\{c_i\}$ are computed by numerically evaluating the above integrals via Gauss quadrature.

It is expected that, by approximately driving the H^1 semi-norm of the functional approximation error to zero, the proposed strategy should effectively arrest the spurious oscillations in the numerical inversion of the Helmholtz equation even if the characteristic particle spacing is coarser than that demanded by the sampling theorem for large wave numbers. In what follows, the interest is in the application of the proposed scheme in computationally feasible simulations of the Helmholtz equation as it appears in the forward model of diffraction tomography, as explained below.

Support of B-spline basis function and bubble function for node I

Support of B-spline basis function and bubble function for node J
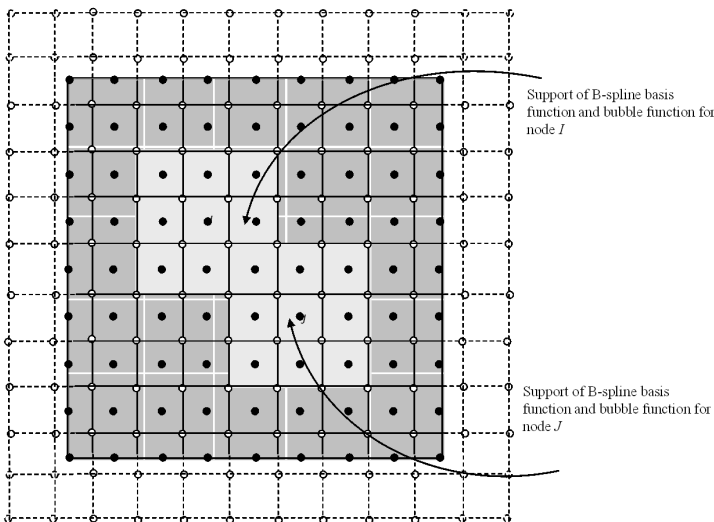
Figure 2: Supports of bubble function and B-spline basis function for nodes I and J

4 Helmholtz equation in diffraction tomography

Diffraction tomography is used to recover properties of the objects such as refractive index from scattered radiation when the spatial resolution required is comparable to the wavelength of radiation used to interrogate the objects. The standard algorithm for refractive index recovery uses the Fourier diffraction theorem (FDT)

which equates the Fourier transform of the scattered amplitude to the Fourier transform of the unknown refractive index, reminiscent of the Fourier slice theorem of X-ray tomography. However the FDT is derived under restrictive approximations on the size of the object and variations of refractive index, either the Born- or Rytov approximation. Even though the Rytov is less restrictive than Born, still the variations of the property is so restricted that the recovery of refractive index with changes expected in the third and second decimal places is quite unsatisfactory using the FDT. Thus one of the important applications of optical tomography which is non-destructive evaluation of optical fiber and optical waveguides is outside the scope of the FDT-based diffraction tomography. In this context an iterative procedure which employs Newton algorithm to minimize the mean-square error between measured scattered field and its computed counterpart is often employed. In the iteration the nonlinear problem is 'locally' linearized and an update equation for the parameter to be recovered is setup and solved. The implementation of this iterative algorithm requires, among other steps, the repeated evaluation of the scattered field by solving the forward propagation model, which is the wave equation, or its time-Fourier transformed version, the Helmholtz equation. It is in the numerical solution of the Helmholtz equation for large values of the propagation vector modulus (i.e. $k(\mathbf{r})$, $\mathbf{r}$ being the position vector) that one faces the greatest challenge *en route* to employing an iterative parameter recovery algorithm. For large k, the solution of the Helmholtz equation suffers from spurious oscillations brought in by the inherent instability (virtual loss of ellipticity) of the discretized system resulting from the Helmholtz equation.

The objects of interest in integrated optics such as optical fiber and optical waveguides, even though the refractive index variation is large enough to violate the assumptions of the Rytov approximation, still come under the category of the so called 'weakly scattering' objects. For such weakly varying refractive index distributions, one neglects the second order term of the inhomogeneous refractive index distribution in $k^2(\mathbf{r})$. In this case it is possible to use an approximate form of Helmholtz equation to represent forward propagation of light, as shown below.

The propagation of monochromatic wave of wavelength λ_0 through a medium of refractive index distribution $\eta(\mathbf{r})$ in a domain shown in Fig. 3 is governed by the Helmholtz equation:

$$\nabla.\nabla u(\mathbf{r}) + k^2(\mathbf{r})u(\mathbf{r}) = 0 \tag{45}$$

The boundary conditions used are:

$$u(\mathbf{r}) = u_{in} \text{ on } L \cup L^- \quad and \tag{46}$$

$$u(\mathbf{r}) + \frac{\partial u(\mathbf{r})}{\partial n} = 0 \text{ on } L^+ \tag{47}$$

where u_{in} is the incident complex amplitude and $\frac{\partial u(\mathbf{r})}{\partial n}$ is the normal derivative of $u(\mathbf{r})$ on L^+.

Here $u(\mathbf{r})$ is the complex scalar amplitude of the wave and k is the modulus of the propagation vector, i.e. $k \equiv |\mathbf{k}| = \eta(\mathbf{r}) \frac{2\pi}{\lambda_0} \equiv \eta(\mathbf{r}).k_0$. Considering $\eta(\mathbf{r}) = 1 + \eta_\delta(\mathbf{r})$, where $\eta_\delta(\mathbf{r})$ is the small perturbation to the background medium whose refractive index is assumed to be one, we write $k(\mathbf{r})$ in terms of $\eta_\delta(\mathbf{r})$ as:

$$k^2(\mathbf{r}) \approx k_0^2(1 + 2\eta_\delta(\mathbf{r})) \tag{48}$$

Using $f(\mathbf{r})$ to denote $-2\eta_\delta(\mathbf{r})$, we can rewrite equation (45) as:

$$\nabla.\nabla u(\mathbf{r}) + k_0^2(1 - f(\mathbf{r}))u(\mathbf{r}) = 0 \tag{49}$$

If $\eta_\delta(\mathbf{r})$ is not small enough for the approximation in equation (48) to hold then the forward model should be Equation (45) which holds for large variations in $\eta(\mathbf{r})$ inside the object. This is the case for optical fibers for which variation in refractive index between the core and cladding is in the first or second decimal place. For certain integrated optics waveguides the refractive index variation is small enough for which the following weak-scattering formulation holds. For objects where the overall k variation is small, the traditional FEM formulation is able to solve the forward equation without appreciable numerical errors. For objects with larger variations, the usual FEM fails because of pollution effects; it is in here our proposed formulation of nearly H^1 optimal mesh-free method gives accurate results (as verified by comparison with experimental data).

For completeness we give a perturbation equation connecting $\eta_\delta(\mathbf{r})$ to $v(\mathbf{r})$, the scattered field under weak scattering approximation. The object, assumed to be 2-D square shaped with boundaries L, L^- and L^+, as shown in Fig. 3 is illuminated with the plane wave $e^{ik_0\mathbf{r}.\theta}$. Here θ is the unit vector in the propagation direction, given by

$$\theta = \begin{bmatrix} -\sin\varphi \\ \cos\varphi \end{bmatrix} \tag{50}$$

where $\mathbf{r} \in \mathbb{R}^2$ and φ is the angle of illumination. The total field $u(\mathbf{r})$ at any point in the medium is given by sum of incident wave $e^{ik_0\mathbf{r}.\theta}$ and the scattered wave $v(\vec{r})e^{ik_0\mathbf{r}.\theta}$ that is

$$u(\mathbf{r}) = e^{ik_0\mathbf{r}.\theta}(1 + v(\mathbf{r})) \tag{51}$$

Here it is assumed that the scattered wave is obtained from the incident wave through a multiplicative perturbation $v(\mathbf{r})$.

Substituting the above expression for $u(\mathbf{r})$ into equation (49), through a small rear-rangement of terms we get the following equation connecting $f(\mathbf{r})$, the perturbation in refractive index to $v(\mathbf{r})$, and the multiplicative perturbation owing to scattering on the incident plane wave.

$$\nabla.\nabla v(\mathbf{r}) + 2ik_0\theta.\nabla v(\mathbf{r}) - k_0^2 f(\mathbf{r})v(\mathbf{r}) = k_0^2 f(\mathbf{r}) \qquad (52)$$

The above equation models the forward propagation of light through the object with the following boundary conditions (see Fig. 3):

$$v(\mathbf{r}) = 0 \quad \text{on } L \cup L^- \quad and \qquad (53)$$

$$v(\mathbf{r}) + \frac{\partial v(\mathbf{r})}{\partial n} = 0 \text{ on } L^+ \qquad (54)$$

where $\frac{\partial v(\mathbf{r})}{\partial n}$ is the normal derivative of $v(\mathbf{r})$ on L^+.
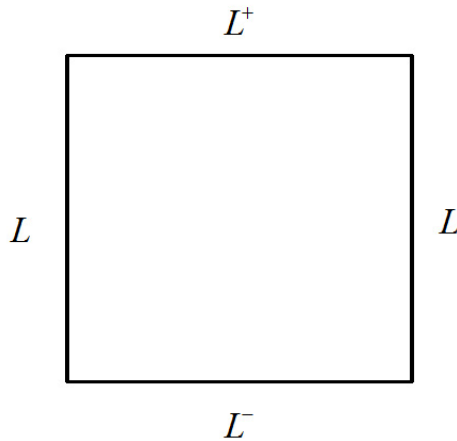
Figure 3: Problem domain

In one of the numerical implementations of the Helmholtz equation, when the $\eta(\mathbf{r})$ variation is small enough to admit the approximation in equation (48), we use the standard (Bubnov-Galerkin) FEM to solve Equations (52)-(54) for $v(\mathbf{r})$ and compute the total field $u(\mathbf{r}) = e^{ik_0\mathbf{r}.\theta}(1+v(\mathbf{r}))$ from which the intensity $I(\mathbf{r}) = u(\mathbf{r})u^*(\mathbf{r})$ and its normal derivative are calculated and compared with the corresponding experimentally measured values. The new H^1 optimal mesh-free scheme is only used when the above approximation fails to hold. Results are discussed in Section 5.

5   Numerical computations and results

5.1   *Numerical computation*

In this section we specifically consider the numerical implementation of the Helmholtz equation with and without the weak scattering approximations. The details of the implementation of weak scattering approximation are given below

For convenience, the variables $v(\mathbf{r})$ and $f(\mathbf{r})$ are decomposed into their real and imaginary parts:

$$v(\mathbf{r}) = v_r(\mathbf{r}) + iv_i(\mathbf{r}) \tag{55}$$

$$f(\mathbf{r}) = f_r(\mathbf{r}) + if_i(\mathbf{r}) \tag{56}$$

In the above equations, while the subscript i is an integer, the coefficient i is given by $i = \sqrt{-1}$. Substituting (55) and (56) into (52), and separating the real and imaginary parts we get:

$$
\begin{aligned}
\nabla^2 v_r(\mathbf{r}) - 2k_0 \frac{\partial v_i(\mathbf{r})}{\partial y} - k_0^2 f_r(\mathbf{r}) v_r(\mathbf{r}) + k_0^2 f_i(\mathbf{r}) v_i(\mathbf{r}) = k_0^2 f_r(\mathbf{r}) \\
\nabla^2 v_i(\mathbf{r}) + 2k_0 \frac{\partial v_r(\mathbf{r})}{\partial y} - k_0^2 f_r(\mathbf{r}) v_i(\mathbf{r}) - k_0^2 f_i(\mathbf{r}) v_r(\mathbf{r}) = k_0^2 f_i(\mathbf{r})
\end{aligned}
\tag{57}
$$

The above system of equations can be written as:

$$\mathbf{LU} = \mathbf{F} \tag{58}$$

where

$$
\mathbf{L} = \left[
\begin{array}{cc}
(\nabla^2 - k_0^2 f_r(\mathbf{r})) & -(2k_0 \frac{\partial}{\partial y} - k_0^2 f_i(\mathbf{r})) \\
(2k_0 \frac{\partial}{\partial y} - k_0^2 f_i(\mathbf{r})) & (\nabla^2 - k_0^2 f_r(\mathbf{r}))
\end{array}
\right]
$$

$$
\mathbf{U} = \left[
\begin{array}{c}
v_r(\mathbf{r}) \\
v_i(\mathbf{r})
\end{array}
\right]
\quad
\mathbf{F} = \left[
\begin{array}{c}
k_0^2 f_r(\mathbf{r}) \\
k_0^2 f_i(\mathbf{r})
\end{array}
\right]
$$

The object domain is a square of size 240μm x240 μm, as shown in Figure 3. The object has a circular inhomogeneity of radius 70μm (in the background refractive index of $(1.472+0i)$), which is at $(0, 0)$ with refractive index varying from 1.4805 to 1.51. With this object, Equation (57) is solved using the standard FEM. These results are verified using the experimentally measured intensity and normal derivative of intensity (for a description of the experiment, see Section 5.2) and shown in Figures 4 and 5 respectively. Since the standard FEM gives results which match well the experimental data, there is no need to use the new H^1 optimal mesh-free
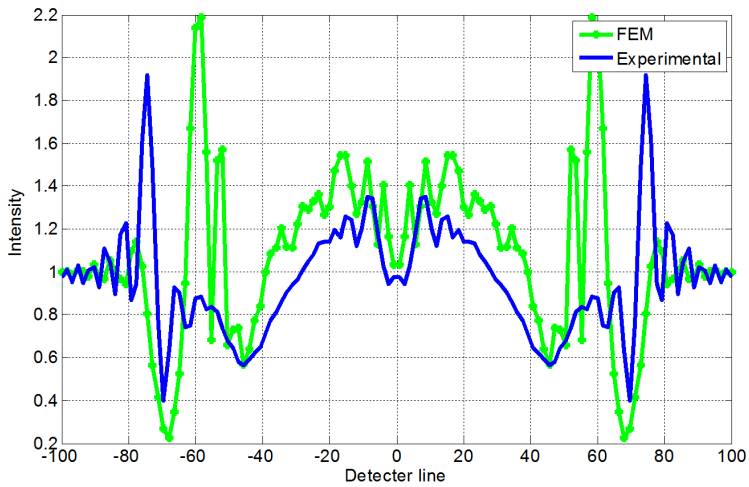
Figure 4: Intensity distribution
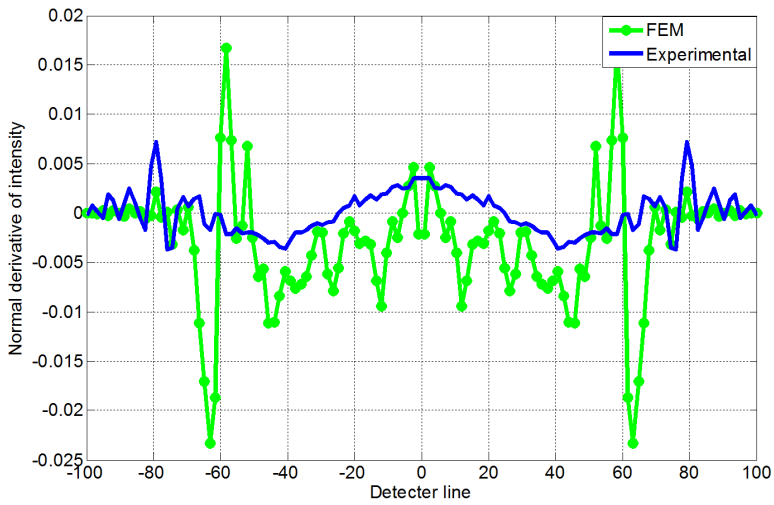
Figure 5: Normal derivative of intensity

method (which is computationally more expensive) to further improve the FEM results.

However, when variation in $\eta(\mathbf{r})$ is large so that Equation (45) is the right forward equation and Equations (52)-(54) do not hold, the traditional FEM fails to give solution. Here we bring in the new formulation and solve Equation (45) using the nearly H^1 optimal Petrov-Galerkin method (Section 3). For details of the numerical simulations and comparison with experimental data see Section 5.3.

5.2 Experiment

The experimental setup is shown in Figure 6. The illumination is from a quasi-monochromatic and spatially incoherent source. This is obtained by sending a He-Ne laser beam (power 10 mW) through a combination of static and rotating diffusers. The beam coming out of the rotating diffuser is collimated by a corrected doublet with collimation checked by a parallel plate interferometer. The collimated spatially incoherent light illuminates the object, which is a 140μm optical fiber stripped off its plastic jacket and immersed in a cuvette containing an index-matching liquid which is anhydrous glycerol with refractive index of 1.472. The transmitted intensity at a plane few hundreds of microns behind the optical fiber is measured using a 14 bit CCD camera (guppypro F031).
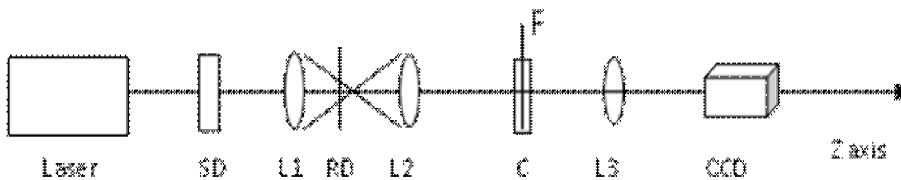
Figure 6: Schematic diagram of experimental set up. The light from the He-Ne laser is send through the static diffuser (SD) and rotating diffuser (RD) to spoil the spatial coherence. This light beam collimated by lenses L1 and L2 falls on the optical fiber(F) immersed in index matching liquid in the cuvette(C).The transmitted light distribution in the planes behind the fiber is magnified using lens L3 and is caught on the CCD.

The normal derivative of intensity (here the normal is along the $z-$axis which is the optic axis of the system) is computed from the recorded intensities around the required output plane by focusing the camera at a number of $x - y$ planes corresponding to a sequence of z-values around the plane of interest. From the recorded

intensities a polynomial expansion of intensity in terms of z is obtained from which the normal derivative of intensity ($\frac{\partial I(x,y,z)}{\partial z}$) is computed.

5.3   Comparison of results

In the next numerical experiment we consider an object (a fiber with larger refractive index variation) for which the restriction imposed on refractive index by Equation (48) is not valid. Hence we model light propagation using the Helmholtz equation in its original form without simplification, which is Equation (45), which is the most appropriate forward model. The boundary conditions are as given in Equations (47-48) and we once again implement the forward equation using the traditional FEM and proposed H^1optimal Petrov-Galerkin mesh-free scheme.

The results, which are the scattered intensity and its normal derivative plots, are shown in Figures (7) and (8). For comparison, experimental results obtained using the set-up of Section 5.2 is also shown. It is clearly seen that the numerical results from the new scheme match the experimental results far better compared to those from the conventional FEM which only results in the trivial solution.
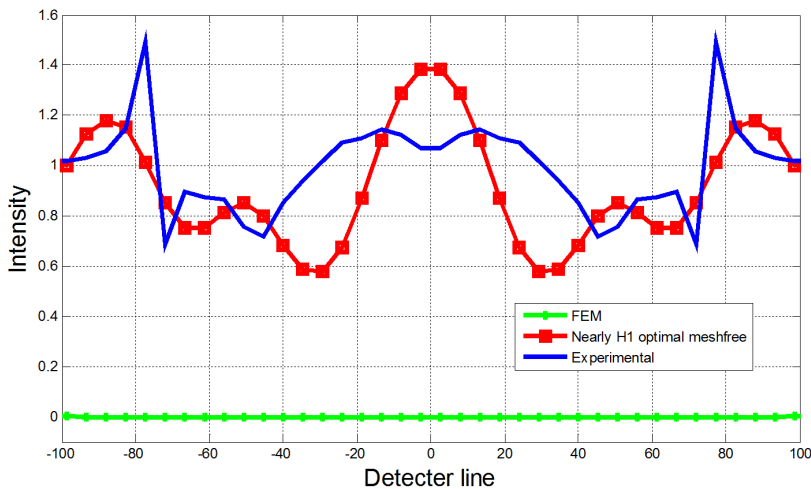
Figure 7: Scattered intensity distribution
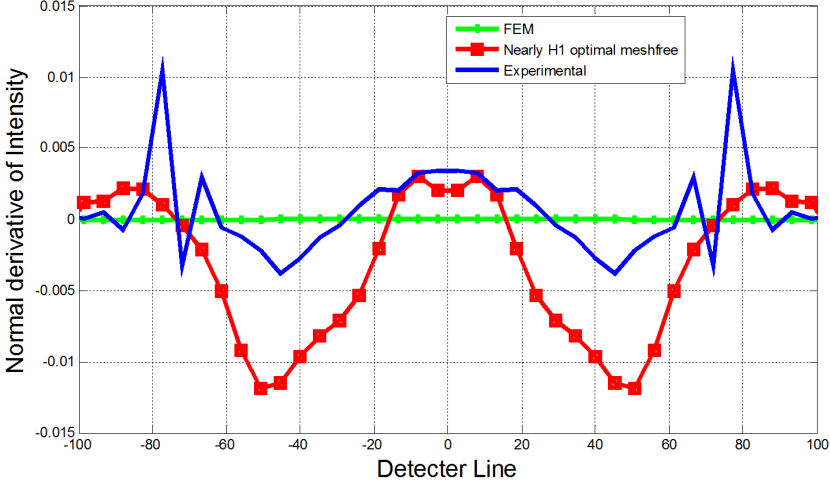
Figure 8: Normal derivative of intensity

6 Conclusions

A Petrov-Galerkin mesh-free method, with B-splines or NURBS as the basis for globally smooth functional approximation, is proposed for approximately incorporating the H^1 optimality criterion in the weak form of the governing PDE and demonstrated for nearly pollution free solution of the Helmholtz equation for relatively large k values. With this the loss of ellipticity in the Helmholtz equation, resulting in both dispersion and pollution effects, is effectively tackled. While a rigorous theoretical justification of this stabilizing effect has been kept beyond the scope of this article, an inspection of the H^1 optimality condition reveals that it indeed behaves as a consistent diffusion term that may be responsible in removing the pollution effects as evidenced through the numerical work. Vis-à-vis the conventional FEM, part of the superior numerical accuracy with the proposed method may also be attributed to the smooth shape functions that satisfy polynomial reproducing conditions and to their normal derivatives being zero on the support boundaries. The method is tested by solving the Helmholtz equation, which is the forward equation of diffraction tomography aiming at recovering refractive index distributions from scattered field. For the sake of comparisons with experiments which generally measure intensity and the normal derivative of intensity, we have computed both these quantities from the scattered field obtained by solving the Helmholtz equation. We have considered the light propagation through refractive index distributions under two conditions: (i) one for which the refractive index variation

are small enough so that a weak-scattering approximation holds and (ii) the second where the above approximation is not valid. In the first case it is shown that the FEM is good enough to discretize and invert the forward equation. In the second case, however, it is shown that the numerical accuracy of solutions from the FEM is grossly inadequate, whereas those from the proposed method are much superior as testified via the pattern matching with the experimental data. One of the missing links in the iterative recovery of refractive index distributions of objects not restricted to be weakly scattering from scattered intensity, which is an accurate 'forward solver' yielding the scattered field with the refractive index distribution as the input, is now made available through the present work.

It seems possible to use the above implementation of H^1 optimality as a generic tool for ellipticization against a possible loss of ellipticity using any mesh-free method, e.g. the MLPG. In addition, the non-hyper-singular intergral equation approach (Qian, Han and Atluri 2013), wherein the boundary integrals in an appropriately reduced non-symmetric weak form are numerically implemented through a fast multilevel multipole algorithm, could also be exploited to arrive at a stable solution of the Helmholtz equation with large wavenumbers. Explorations of such approaches to stabilize numerical solutions of impact dynamical systems in the softening plasticity regime (based on, say, a gradient plasticity theory) could also constitute an interesting aspect of future research.

Appendix I

1. B-splines, NURBS and geometric modeling via NURBS

For completeness in the description of the algorithm needed whilst numerically implementing the H^1 optimal ERKM, a brief introduction to B-spline basis functions, curves and surfaces would be in order. For a more detailed account, see Piegl and Tiller (1997).

1.1 B-splines

B-splines constitute a generalization of Bézier curves. The recursive definition of the ith normalized B-spline basis functions of degree p(order p +1) is given by:

$$R_i^p(\xi) = \begin{cases} 1 & \text{if } \xi_i \leq \xi \leq \xi_{i+1} \\ 0 & \text{otherwise} \end{cases} \tag{59}$$

$$R_i^p(\xi) = \frac{\xi - \xi_i}{\xi_{i+1} - \xi_i} R_i^{p-1}(\xi) + \frac{\xi_{i+p+1} - \xi}{\xi_{i+p+1} - \xi_{i+1}} R_{i+1}^{p-1}(\xi), \quad i = 1, 2, 3, ...n + p + 1 \tag{60}$$

where $\Xi = \{\xi_1, \xi_2, \xi_3........\xi_{n+p+1} | \xi_i \in \mathbf{R}\}$ is a non-decreasing sequence of real scalars, defined over a parametric space and referred to as the knot vector, p the degree of the polynomial (appearing in the numerators) and n the number of basis functions. In the above definition, 0/0 (whenever it occurs) must be replaced by 0. Knots are called uniform if they are equally spaced. In the parametric space, knots can be repeated at the same coordinate. A knot vector is 'open' if its first and last knots appear $p+1$ times. Basis functions in one dimension formed via open knot vectors are interpolating at the boundary of the parametric domainΞ. Although $R_i^p(\xi)$ is defined everywhere on the real line, it has non-zero values only in the interval$[\xi_i, \xi_{i+p+1})$. An example of a cubic basis function for a uniform knot vector (open and closed) is presented in Figure 9.

(a)　　　　　　　　　　　　　　(b)
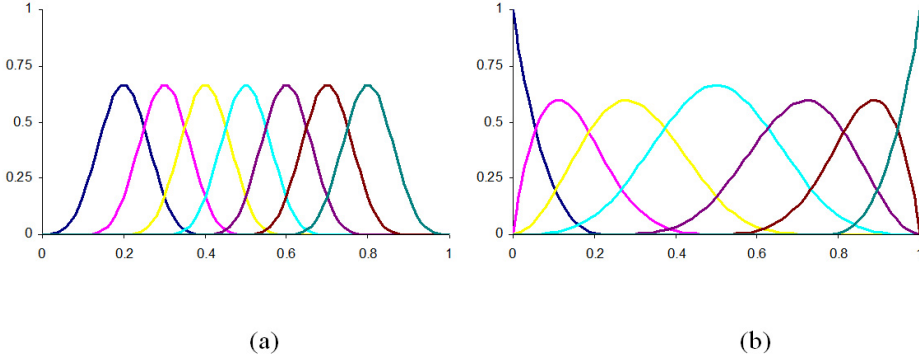
Figure 9: The cubic B-spline basis function for
(a) uniform knot vector $\Xi = \{0, 0.1, 0.2, 0.3, 0.4, 0.5, 0.6, 0.7, 0.8, 0.9, 1.0\}$
(b) open uniform knot vector $\Xi = \{0, 0, 0, 0, 0.25, 0.5, 0.75, 1.0, 1.0, 1.0, 1.0\}$

A few salient properties of B-spline basis functions are summarized below.

1. **Local support property**: $R_i^p(\xi) = 0$ if ξ is outside the interval $[\xi_i, \xi_{i+p+1})$. In any given knot span, $[\xi_i, \xi_{i+1})$, at most $p+1$ of $R_i^p(\xi)$ are nonzero, namely the functions $R_{j-p}^p, ..., R_j^p$. For example, the only cubic non-zero functions on $[\xi_3, \xi_4)$ are $R_0^3, ..., R_3^3$.

2. **Non-negativity:** $R_i^p(\xi) \geq 0 \forall i, p, \xi$

3. **Partition of unity:** For an arbitrary knot span $[\xi_i, \xi_{i+1})$, $\sum\limits_{j=i-p}^{i} R_j^p(\xi) = 1 \quad \forall \xi \in [\xi_i, \xi_{i+1})$

4. All derivatives of $R_i^p(\xi)$ exist in the interior of a knot span. At a knot, $R_i^p(\xi)$ is $p - k$ times continuously differentiable, where k is the multiplicity of the knot. Hence increasing the degree increases continuity and increasing the knot multiplicity decreases continuity.

5. Except for $p = 0$, $R_i^p(\xi)$ attains exactly one maximum value.

1.2 B-spline curves

Using the B-spline basis function, B-spline curves may be constructed as:

$$C(\xi) = \sum_{i=1}^{N_P} R_i^p(\xi) P_i \tag{61}$$

where R_i^p is the ith B-spline basis function of degree p, P_i are the coefficients of B-spline basis functions, called control points, and N_P is the number of control points. The polygon formed by $\{P_i\}$ is called the control polygon. In general control points are not interpolated by B-spline curves. A cubic B-spline curve on an open uniform knot (Figure 9(b)) is shown in Figure 10.
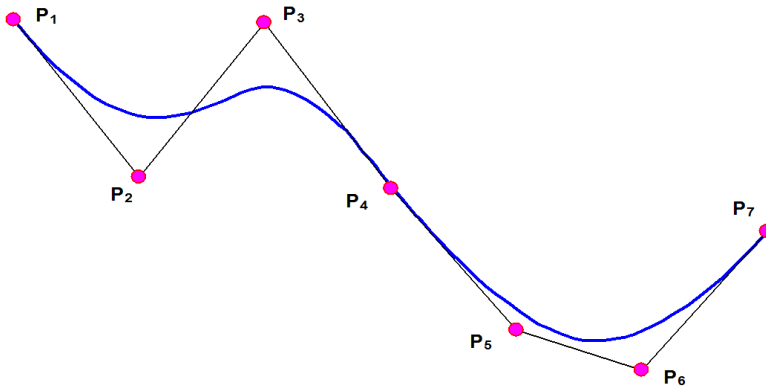
Figure 10: A cubic B-spline curve on an open uniform knot vector $\Xi = \{0, 0, 0, 0, 0.25, 0.5, 0.75, 1.0, 1.0, 1.0, 1.0\}$, basis functions are shown in Figure 9(b)

1.3 B-splines in Higher Dimensions:

Higher dimensional B-spline basis function may be constructed by taking the tensor product of B-spline basis functions in one dimension.

B-spline Surfaces

A B-spline surface is obtained by taking a bidirectional net of control points, two knot vectors and the products of univariate B-spline functions:

$$S(\xi, \eta) = \sum_{i=1}^{N_{P_\xi}} \sum_{j=1}^{N_{P_\eta}} R_i^p(\xi) R_j^q(\eta) P_{ij} \tag{62}$$

$R_i^p(\xi)$ and $R_j^q(\eta)$ are two different sets of one dimensional B-spline basis functions of orders p and q respectively. Moreover, they are defined on the knot vectors $\Xi = \{\xi_1, \xi_2, \xi_3......\xi_{n+p+1} | \xi_i \in R\}$ and $\overline{\Xi} = \{\eta_1, \eta_2, \eta_3......\eta_{n+q+1} | \eta_i \in R\}$ respectively. Note that $\{P_{ij}\}$, $i = 1, 2, ...N_{P\xi}$ and $j = 1, 2, ...N_{P\eta}$, defines the control net.

1.4 B-spline solids:

B-spline solids are defined in a fashion analogous to the definition of B-spline surfaces. Given a control net $\{P_{ijk}\}$, $i = 1, 2, ...N_{P\xi}$, $j = 1, 2, ...N_{P\eta}$, $j = 1, 2, ...N_{P\varsigma}$ and knot vectors $\Xi = \{\xi_1, \xi_2, \xi_3......\xi_{n+p+1} | \xi_i \in \mathbf{R}\}$, $\overline{\Xi} = \{\eta_1, \eta_2, \eta_3......\eta_{n+q+1} | \eta_i \in \mathbf{R}\}$ and $\tilde{\Xi} = \{\varsigma_1, \varsigma_2, \varsigma_3......\varsigma_{n+r+1} | \varsigma_i \in \mathbf{R}\}$, a B-spline solid is defined as:

$$S(\xi, \eta, \varsigma) = \sum_{i=1}^{N_{P_\xi}} \sum_{j=1}^{N_{P_\eta}} \sum_{k=1}^{N_{P_\varsigma}} R_i^p(\xi) R_j^q(\eta) R_j^r(\varsigma) P_{ijk} \tag{63}$$

1.5 The non-uniform rational B-spline (NURBS):

The rational basis function in one dimension is defined as:

$$\bar{R}_i^p(\xi) = \frac{R_i^p(\xi) w_i}{\sum\limits_{k=1}^{N_P} R_k^p(\xi) w_k} \tag{64}$$

R_i^p is the ith B-spline basis function of degree p and w_i is the weight associated with the ith control point P_i. Similarly, in 2 and 3 dimensions, NURBS basis functions are given by:

$$\bar{R}_i^p(\xi, \eta) = \frac{R_i^p(\xi) R_j^p(\eta) w_{ij}}{\sum\limits_{\hat{i}=1}^{N_{P_\xi}} \sum\limits_{\hat{j}=1}^{N_{P_\eta}} R_{\hat{i}}^p(\xi) R_{\hat{j}}^p(\eta) w_{\hat{i}\hat{j}}} \tag{65}$$

$$\bar{R}_{i,j,k}^p(\xi, \eta, \varsigma) = \frac{R_i^p(\xi) R_j^p(\eta) R_k^p(\varsigma) w_{ijk}}{\sum\limits_{\hat{i}=1}^{N_{P_\xi}} \sum\limits_{\hat{j}=1}^{N_{P_\eta}} \sum\limits_{\hat{k}=1}^{N_{P_\varsigma}} R_{\hat{i}}^p(\xi) R_{\hat{j}}^p(\eta) R_{\hat{k}}^p(\varsigma) w_{\hat{i}\hat{j}\hat{k}}} \tag{66}$$

References

Atluri, S. N.; Han, Z. D.; Rajendran, A. M. (2004): A new implementation of the meshless finite volume method, through the MLPG "mixed" approach. *Computer Modeling in Engineering & Sciences,* vol. 6, no. 6, pp. 491 – 513.

Atluri, S. N.; Zhu, T. (1998): A new meshless local Petrov-Galerkin (MLPG) approach in computational mechanics. *Computational Mechanics,* vol. 22, pp. 117-127.

Babuska, I.; Ihlenburg, F.; Paik, E.; Sauter, S. A. (1995): A generalized Finite element method for solving the Helmholtz equation in two dimensions with minimal pollution. *Computer Methods in Applied Mechanics and Engineering*, vol. 128, no. 3-4, pp. 325-359.

Babuska, I.; Melenk, J. M. (1997): The partition of unity method. *International Journal for Numerical Methods in Engineering*, vol. 40, no. 4, pp.727–758.

Babuška, I.; Sauter, S. A. (2000): Is the pollution effect of the FEM avoidable for the Helmholtz equation considering high wave number? *SIAM Rev.*, vol. 42, no. 3, pp. 451–484.

Bao, G.; Wei, G. W.; Zhao, S. (2004): Numerical solution of the Helmholtz equation with high wave number. *International Journal for Numerical Methods in Engineering*, vol. 59, no. 3, pp. 389-408.

Bao, G.; Wei, G. W.; Zhao, S. (2004): Numerical modeling of electromagnetics via a wavelet-collocation method. *Antennas and propagation society International Symposium, IEEE,* vol. 2, pp.1467-1470

Barbone, P. E.; Harari, I. (2001): Nearly H1-optimal finite element methods. *Computer Methods in Applied Mechanics and Engineering* vol. 190, no. 43, pp. 5679–5690.

Brezzi, F.; Franca, L. P.; Russo, A. (1998): Further considerations on residual-free bubbles for advective–diffusive equations. *Advances in Stabilized Methods in Computational Mechanics*, vol. 166, no. 1–2, pp. 25–33.

Brooks, A. N.; Hughes, T. J. R. (1982): Streamline upwind/Petrov–Galerkin formulations for convection dominated flows with particular emphasis on the incompressible Navier-Stokes equations. *Computational Methods in Applied Mechanics and Engineering,* vol. 32, pp. 199–259.

Bruno, O.; Geuzaine, C.; Reitich, F. (2004): A new high-order high-frequency integral equation method for the solution of scattering problems I: Single-scattering configurations. *Proceedings of the 20th Annual Review of Progress in Applied Computational Electromagnetics, ACES,* vol. 20,

Chen,J. S.; Pan, C.; Wu, T. C.; Liu, W.K. (1996): Reproducing kernel particle

methods for large deformation analysis of non-linear structures. *Computer Methods in Applied Mechanics and Engineering*, vol. 139, no. 1-4, pp. 195–227.

Devaney, A. J. (1982): A filtered back propagation algorithm for diffraction tomography. *Ultrasonic Imaging,* vol. 4, no.4, pp. 336-350.

Duarte, C.A.; Oden, J. T. (1996): An h-p adaptive method using clouds. *Computer Methods in Applied Mechanics and Engineering,* vol. 139, no. 1, pp. 237–262.

Farhat, C.; Harari, I.; Franca, L. P. (2001): The discontinuous enrichment method. *Computer Methods in Applied Mechanics and Engineerin,* vol. 190, no. 48, pp. 6455–6479.

Franca, L.P.; Nesliturk, A.; Stynes, M. (1998): On the stability of residual-free bubbles for convection-diffusion problems and their approximation by a two-level finite element method. *Computer Methods in Applied Mechanics and Engineering,* vol. 166, no. 1–2, pp. 35–49.

Harari, I.; Hughes, T. J. R. (1992): Galerkin/ least-squares finite element methods for the reduced wave equation with non-reflecting boundary conditions in unbounded domains. *Computer Methods in Applied Mechanics and Engineering,* vol. 98, no. 3, pp. 411–454.

Ihlenburg, F, Babuška, I. (1997): Finite element solution of the Helmholtz equation with high wave number part II: the $h - p$-version of the FEM. *SIAM Journal on Numerical Analysis*, vol. 34, no. 1, pp. 315–358.

Ihlenburg, F.; Babuska, I. (1995): Dispersion analysis and error estimation of Galerkin Finite element methods for the Helmholtz equation. *International Journal for Numerical Methods in Engineering*, vol. 38, no. 22, pp. 3745-3774.

Ihlenburg, F.; Babuška, I. (1995): Finite element solution of the Helmholtz equation with high wavenumber part I: the h-version of the FEM. *Computers & Mathematics with Applications*, vol. 30, no. 9, pp. 9–37.

Liu, W. K., Jun, S., Zhang, Y. F. (1995): Reproducing kernel particle methods, *International Journal for Numerical Methods in Fluids*, vol. 20, pp.1081–1106.

Liu, G. R.; Gu, Y. T. (2001): A point interpolation method for two-dimensional solids. *International Journal for Numerical Methods in Engineering,* vol. 50, no. 4, pp. 937–951.

Liu, W. K.; Jun, S.; Li, S.; Adee, J.; Belytschko, T. (1995): Reproducing kernel particle methods for structural dynamics. *International Journal for Numerical Methods in Engineering*, vol. 38, no. 10, pp. 1655–1679.

Liu, W. K.; Li, S.; Belytschko, T. (1997): Moving least square reproducing kernel methods (I) methodology and convergence. *Computer Methods in Applied Me-*

chanical Engineering, vol. 143 no. 1-2, pp. 113–154.

Lu, Y. Y.; Belytschko, T.; Gu, L. (1994): A new implementation of the element free Galerkin method. *Computer Methods in Applied Mechanics and Engineering*, vol. 113, no. 3-4, pp. 397–414.

Melenk, J. M.; Babuska, I. (1996): The partition of unity finite element method: basic theory and applications. Computer *Methods in Applied Mechanics and Engineering,* vol. 139, no. 1-4, pp. 289–314.

Monk, P.; Wang, D. (1999): A least-squares method for the Helmholtz equation. *Computer Methods in Applied Mechanics and Engineering*, vol. 175, no. 1-2, pp. 121-136.

Natterer, F.; Wubbeling, F. (2005): Marching schemes for inverse acoustic scattering problems. Journal of Numerische Mathematik, vol. 100, no. 4, pp. 697–110.

Oberai, A. A.; Pinsky, P. M. (2000): A residual-based finite element method for the Helmholtz equation. *International Journal for Numerical Methods in Engineering,* vol. 49, no. 3, pp. 399–419.

Piegl, L.; Tiller, W. (1997): The NURBS Book, *Springer, Berlin.* pp. 43–69.

Qian, Z. Y.; Han, Z. D.; Ufimtsev, P.; Atluri, S. N. (2004): Non-hyper-singular boundary integral equations for acoustic problems, implemented by the collocation based on boundary element method. Cmes - Computer Modeling in Engineering & Sciences, vol. 6, no. 2, pp. 133–144.

Qian, Z. Y.; Han, Z. D. and Atluri, S. N. (2013): A fast regularized boundary integral method for practical acoustic problems. Cmes - Computer Modeling in Engineering & Sciences,vol. 91, no.6, pp. 133–144.

Shaw, A.; Banerjee, B., Roy, D. (2008): A NURBS-based method parametric bridging mesh free and finite element formulations. *Computer Modeling in Engineering & Sciences* vol. 26, no. 1 pp. 31–60

Shaw, A.; Bendapudi, A., Roy, D. (2008): A Kriging-based Error Reproducing and Interpolating Kernel Method for Improved Mesh-free Approximations. International *Journal for Numerical Methods in Engineering*, vol. 73, no. 10, pp. 1434-1467.

Shaw, A.; Roy, D. (2007): A novel form of reproducing kernel interpolation method with applications to nonlinear mechanics. *Computer Modeling in Engineering & Sciences,* vol. 19, no. 1, pp. 69–98.

Shaw, A.; Roy, D. (2007): A NURBS-based error reproducing kernel method with applications in solid mechanics. *Computational Mechanics*, vol. 40, no. 1, pp. 127–148.

Shaw, A.; Roy, D. (2008): NURBS-based Parametric Mesh-free Methods. *Com-*

puter methods in Applied Mechanics and Engineering vol. 197, no. 17-18, pp. 1541- 1567.

Strouboulis, T.; Babuska, I., Copps, K. (2000): The design and analysis of the generalized finite element method. *Computational Methods in Applied Mechanical Engineering*, vol. 181, no. 1–3, pp. 43-69.

Sunilkumar, N.; Roy, D. (2010): A smooth finite element method based on reproducing kernel DMS-splines. *Computer Modeling in Engineering & Sciences,* vol. 65, no. 2, pp. 107-153

Sunilkumar, N.; Roy, D. (2010): The reproducing kernel DMS-FEM: 3D shape functions and applications to linear solid mechanics, *Computer Modeling in Engineering & Sciences,* vol. 66 no. 3 pp. 249-284.

Sunilkumar, N.; Roy, D., Reid, S. R. (2012): Smooth DMS-FEM: A new Approach for Solving Nearly Incompressible Nonlinear Elasto-Static Problems. *International Journal of Mechanical Sciences.* vol. 54, no. 1, pp. 136-155.

Sunilkumar, N.; Roy, D., Reid, S. R.; Vasu, R. M. (2012): Wrinkled and slack membranes: nonlinear 3D elasticity solutions via smooth DMS-FEM and experiment. *International Journal for Numerical Methods in Engineering,* vol. 90, no. 10, pp. 1233-1260.

Swegle, J. W.; Hicks D. L.; Attaway, S. W. (1995): Smoothed particle hydrodynamics stability analysis. *Journal of Computational Physics,* vol. 116, no. 1, pp. 123–134.

Menke, W. (1984): The resolving power of cross-borehole tomography. *Geophysical Research Letters,* vol. 11, no. 2, pp. 105–108.

Zienkiewicz, O. C. (2000): Achievements and some unsolved problems of the finite element method. *International Journal for Numerical Methods in Engineering.* vol. 47, no. 1-3, pp. 9–28.